ACS Photonics

Article

Cite This: ACS Photonics 2018, 5, 1786−1793

Polarization-Dependent Second Harmonic Diffraction from Resonant GaAs Metasurfaces

Franz J. F. Löchner,[*,†] Anna N. Fedotova,[†,‡] Sheng Liu,[§] Gordon A. Keeler,[§] Gregory M. Peake,[§] Sina Saravi,[†] Maxim R. Shcherbakov,[‡,∥] Sven Burger,[⊥,#] Andrey A. Fedyanin,[‡] Igal Brener,[§] Thomas Pertsch,[†] Frank Setzpfandt,[†] and Isabelle Staude[†]

[†]Institute of Applied Physics, Abbe Center of Photonics, Friedrich Schiller University Jena, 07745 Jena, Germany

[‡]Faculty of Physics, Lomonosov Moscow State University, Moscow 119991, Russia

[§]Center for Integrated Nanotechnologies, Sandia National Laboratories, Albuquerque, New Mexico 87185, United States

[∥]School of Applied and Engineering Physics, Cornell University, Ithaca, New York 14853, United States

[⊥]JCMwave, 14050 Berlin, Germany

[#]Zuse Institute Berlin, 14195 Berlin, Germany

Supporting Information

ABSTRACT: Resonant semiconductor metasurfaces are an emerging versatile platform for nonlinear photonics. In this work, we investigate second-harmonic generation from metasurfaces consisting of two-dimensional square arrays of gallium arsenide nanocylinders as a function of the polarization of the fundamental wave. To this end, we perform nonlinear second harmonic microscopy, where the pump wavelength is tuned to the resonances of the metasurfaces. Furthermore, imaging the generated nonlinear signal in Fourier space allows us to analyze the spatial properties of the generated second harmonic. Our experiments reveal that the second harmonic is predominantly emitted into the first diffraction orders of the periodic arrangements, and that its intensity varies with the polarization angle of the fundamental wave. While this can be expected from the structure of the GaAs nonlinear tensor, the characteristics of this variation itself are found to depend on the pump wavelength. Interestingly, we show that the metasurface can reverse the polarization dependence of the second harmonic with respect to an unstructured GaAs wafer. These general observations are confirmed by numerical simulations using a simplified model for the metasurface. Our results provide valuable input for the development of metasurface-based classical and quantum light sources based on parametric processes.

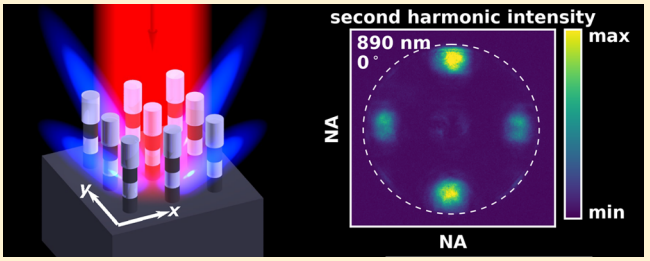

KEYWORDS: *nonlinear metasurfaces, Mie-resonances, nanophotonics, second-harmonic generation, all-dielectric nanophotonics, nonlinear Fourier imaging*

Metasurfaces composed of designed high-refractive-index semiconductor nanoparticles supporting electric and magnetic multipolar Mie-type resonances offer unique opportunities for controlling the properties of light fields transmitted through them or reflected from them.[1,2] Importantly, they can exhibit very low losses for operation frequencies below the fundamental electronic bandgap energy of the respective constituent semiconductor material. Such metasurfaces can, for example, impose a spatially variant phase shift onto an incident light field, thereby providing control over its wavefront with high transmittance efficiency.[3−6]

However, most semiconductor metasurfaces realized so far were studied in the regime of linear optics. More recently, a growing amount of research is concentrating on the nonlinear optical properties of resonant semiconductor metasurfaces. This research has already demonstrated that semiconductor metasurfaces, as well as their individual building blocks, provide an efficient platform for enhancing and manipulating various nonlinear optical effects. These include third-harmonic generation (THG),[7−9] second-harmonic generation (SHG),[10−13] two-photon absorption,[14,15] and higher-order nonlinear frequency generation and mixing processes,[16−19] as well as intensity dependent refractive index[15,20] and photon acceleration.[21] Coherent processes are of particular interest in the context of spatially varying metasurfaces, as they enable the generation of nonlinear light fields with tailored wave fronts. This was previously shown for plasmonic metasurfaces.[22,23] However, the nonlinear conversion efficiencies of plasmonic

Special Issue: Ultra-Capacity Metasurfaces with Low Dimension and High Efficiency

Received: December 14, 2017
Published: March 14, 2018

DOI: 10.1021/acsphotonics.7b01533
ACS Photonics 2018, 5, 1786−1793

metasurfaces are rather low, on the order of 10^{-11} for THG,[24] and their high absorption losses are a major disadvantage. In contrast, in addition to exhibiting low absorption losses, semiconductor metasurfaces can reach THG (SHG) conversion efficiencies of up to 10^{-6} (10^{-4}).[9,11]

The strong nonlinear-optical response of semiconductor metasurfaces arises from the near-field enhancement inside the high-refractive index semiconductor nanoparticles when excited resonantly in combination with the strong second-order (for noninversion-symmetric semiconductor crystal structure) and third-order (for both inversion-symmetric and noninversion-symmetric crystal structure) nonlinear susceptibilities of constituent semiconductor materials. Additionally, and more intriguingly, the design of the nanoresonators and their in-plane arrangement offer many degrees of freedom for engineering both the near-field and far-field patterns of the metasurfaces. For instance, control of the near-field components of the excitation light field allows for accessing the strong second-order nonlinear susceptibilities of III−V compound semiconductors such as gallium arsenide (GaAs),[12,25−28] aluminum gallium arsenide (AlGaAs),[10,11] or gallium phosphide.[29] Their nonlinear susceptibility tensor features only off-diagonal components ($\chi^{(2)}_{ijk} \neq 0$ for $i \neq j \neq k$ otherwise zero),[30] which can be very large, but are not suited for efficient SHG in bulk materials. In addition to the usual phase matching challenge in bulk nonlinear materials, for III−V semiconductors having a zincblende lattice structure and the mentioned nonlinear tensor structure, excitation of a (100) cut wafer at normal incidence only induces a nonlinear polarization, which generates an electric dipole radiating perpendicular to the excitation. Moreover, for SHG frequencies exceeding the electronic bandgap energy of the GaAs, the generated SHG is efficiently absorbed inside bulk GaAs, leading to a vanishing SHG signal. The complex local field structure of designed nanoresonators and their subwavelength dimensions offer a promising route to overcome these problems. Furthermore, engineering of the radiation patterns of the nanoresonators at the generated nonlinear frequency provides control of the direction into which the nonlinearly generated wave is emitted. This was demonstrated both theoretically[31] and experimentally[11] for SHG from individual nanoresonators. The polarization of the emitted second-harmonic field[11,32] and the dependence of the SHG signal on the polarization of the pump field[32,33] were also studied.

While previous research has clearly demonstrated that Mie-resonant III−V semiconductor metasurfaces are promising candidates for the efficient and controlled generation of tailored nonlinear light fields with near-infrared to visible conversion efficiencies on the order of 10^{-5},[12] a deeper understanding of the experimental factors governing nonlinear frequency generation in such metasurfaces is highly desirable. Importantly, with respect to prior studies performed for single, isolated nanoresonators,[11] the periodic arrangement in the metasurfaces adds additional complexity to the already complex system characterized by tensorial nonlinear susceptibilities and a resonant mode structure. As a first important consequence of the periodic arrangement, semiconductor metasurfaces with Mie-resonances at the pump frequency show diffractive behavior at the SHG and THG frequencies. This is essentially unavoidable due to the typical dimensions of the resonators, which impose minimum requirements for the choice of the lattice constant. As a second consequence for the case of highly symmetric nanoresonators such as nanocylinders, the overall symmetry of the nanostructure will be reduced by the periodic arrangement. This can be expected to introduce an additional source of polarization dependence of the nonlinear optical response. However, none of these effects was systematically studied so far.

Here we experimentally investigate, for the first time to our knowledge, the spatial emission characteristics and pump polarization dependence of SHG from metasurfaces composed of gallium arsenide nanocylinders excited at the spectral position of their fundamental electric and magnetic dipolar Mie-type resonances. Using Fourier imaging, we show that the generated second harmonic is predominantly emitted into the first diffraction orders of the periodic array. We furthermore study the nonlinear signal emitted into the different diffractive channels as a function of the excitation polarization, revealing a sensitive dependence, which varies with excitation wavelength. Most importantly, we identify experimental conditions for which the polarization dependence of the SHG efficiency is fundamentally changed with respect to a bulk wafer structure.

Finally, using a simplified model for our experimental structure, we perform numerical calculations in the undepleted pump approximation of the SHG emitted into the different diffraction orders of the metasurface, reproducing our main observations.

RESULTS AND DISCUSSION

GaAs Metasurface. A sketch of the metasurface geometry and experimental setting is shown in Figure 1a. Fabrication

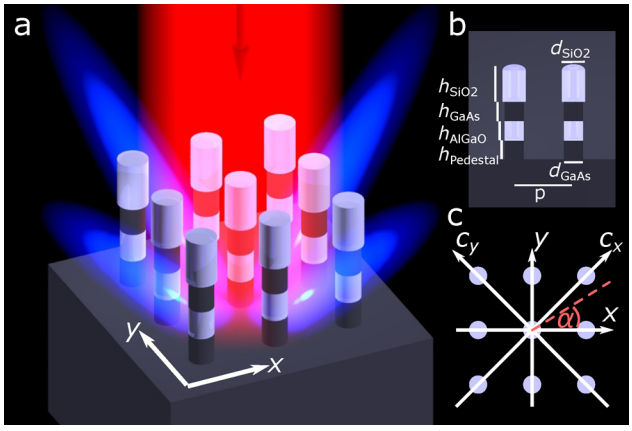

Figure 1. (a) An artist's rendition of the experiment, illustrating excitation and emission of SHG by the investigated metasurface. (b) Cross-sectional sketch of the considered structure showing the definitions of its geometrical parameters. (c) Top view: Orientation of the (010) and (001) crystal directions of the GaAs wafer, indicated by c_x and c_y, with respect to the metasurface lattice directions x and y. Additionally, the orientation of the pump polarization defined by the angle α is indicated.

starts with molecular beam epitaxial growth of a AlGaAs/GaAs stack on top of a semi-insulating (100)-oriented GaAs substrate. Next, single-crystalline GaAs nanocylinders are defined using electron-beam lithography, inductively coupled-plasma etching, and selective oxidization of the $Al_xGa_{1-x}As$ layers to $(Al_xGa_{1-x})_2O_3$[28,34] (see Methods section for fabrication details). Our metasurface has the following geometry parameters as shown in Figure 1b: $d_{GaAs} = d_{AlGaO} = d_{pedestal} = 244$ nm, $h_{GaAs} = h_{pedestal} = 290$ nm, $h_{AlGaO} = 280$ nm, $d_{SiO2} = 296$ nm, $h_{SiO2} = 470$ nm. The sample footprint is

DOI: 10.1021/acsphotonics.7b01533
ACS Photonics 2018, 5, 1786−1793

approximately 700 μm × 700 μm. The fabricated metasurface is designed to support electric and magnetic dipolar Mie-type resonances in the 870−1040 nm wavelength range, bounded by the absorption edge of GaAs and the longest wavelength accessible with our excitation laser system. The lattice period is 755 nm, assuring that the structure does not diffract the excitation wavelengths in the near-infrared spectral range. For the corresponding second-harmonic (SH) wavelengths, in contrast, additional first order diffraction occurs.

The GaAs substrate is oriented in the (100)-direction, and the directions of the crystalline (010)- and (001)-axes are indicated in Figure 1c by the c_x and c_y directions, respectively. These crystalline axes are oriented at 45° with respect to the x- and y-coordinate axes of the rectangular periodic structure of the metasurface. The polarization direction of the linearly polarized excitation beam at the fundamental harmonic (FH) frequency, whose influence we study in this work, is defined via the angle α with respect to the x-direction, as also indicated in Figure 1c.

A scanning electron microscopy (SEM) image of the fabricated metasurface is depicted in Figure 2a, where the

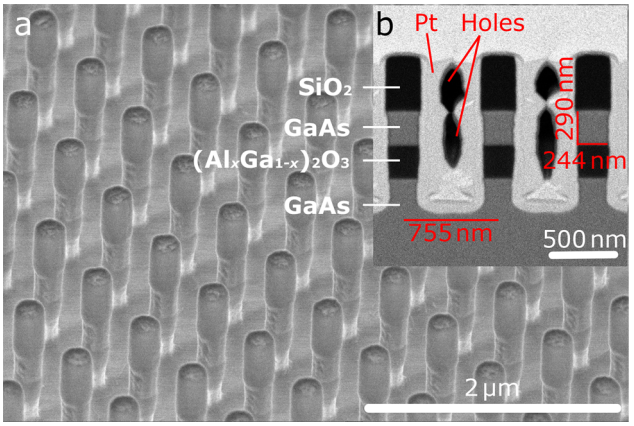

Figure 2. (a) SEM image of a typical fabricated metasurface. (b) Cross-section SEM image revealing the different layers of the structure.

inset in Figure 2b shows a cross-section image of the structure prepared by focused-ion-beam (FIB) milling. A platinum cover layer is applied for FIB milling to increase the contrast, but it is not present for the optical experiments. The GaAs nanocylinders are sandwiched between an SiO_2 cap on the top and a $(Al_xGa_{1-x})_2O_3$ pedestal on the bottom. Additionally, due to overetching, an additional GaAs pedestal is formed below the oxide layer.

As a first step, to characterize the linear-optical properties of the fabricated metasurface we measure reflection spectra for input polarization angles α = 0° and α = 90° using a Fourier-transform infrared spectrometer (Bruker VERTEX 80v) attached to an infrared microscope (Hyperion 2000) with an NA = 0.10 objective. A tungsten halogen lamp was used as a light source. All measured spectra were referenced to corresponding reflection spectra of a silver mirror. The results are displayed in Figure 3a. For both polarizations, we can identify three distinct resonances at 890, 970, and 1030 nm. While the resonance at 890 nm shows the same level of reflectivity for both orthogonal polarizations, the metasurface exhibits pronounced anisotropic behavior at larger wavelengths, including the resonance wavelengths of 970 and 1030 nm. This

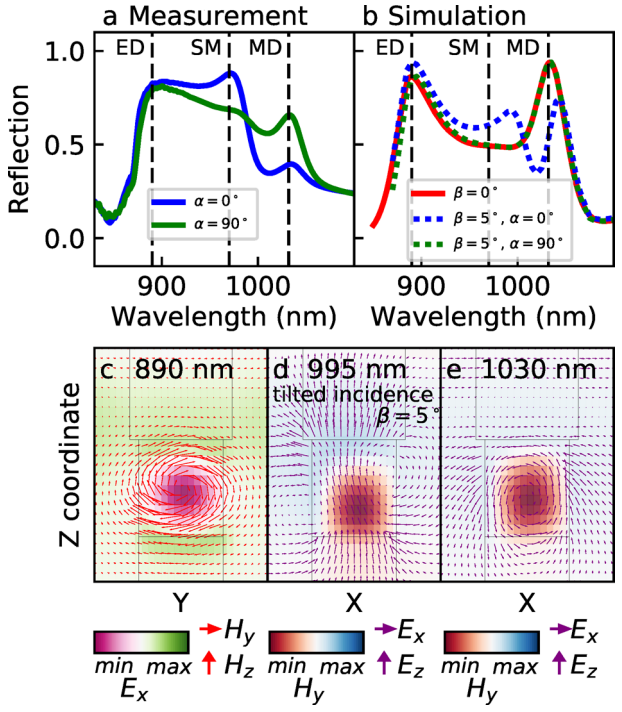

Figure 3. (a) Measured linear-optical reflection spectrum of the investigated metasurface sample for two orthogonal linear input polarizations (α = 0° and α = 90°). The black dashed lines indicate the electric dipole (ED) resonance, the symmetry-forbidden mode (SM), and the magnetic dipole (MD) resonance. (b) Corresponding numerically calculated reflection spectra for normal-incidence and oblique incidence with incidence angle β = 5°. (c−e) Calculated near-field profiles showing cross sections ((y,z) for (c) and (x,z) for (d) and (e)) through the center of the GaAs disk: (c) magnetic y- and z-components (red arrows) and the electric x-component (background coloring) for the resonance at 890 nm, (d, e) electric x- and z-components (purple arrows) and the magnetic y-component (background coloring) for the resonances at 995 nm (β = 5°) and 1030 nm, respectively.

anisotropy is likely due to a slight asymmetry in the fabricated structure.

To compare our measured reflectance spectra with theory, we performed numerical simulations using a time-harmonic finite-element method.[35,36] In our model, we considered a periodic unit cell of the full complex layer stack, illuminated with plane waves in a wavelength range between 850 and 1100 nm. Geometrical parameters are obtained from FIB cross section images of the experimental samples (see Figure 2b). For the refractive indices of the materials we used: literature values for the GaAs,[37] and nondispersive constant values of 1.60 for the oxide AlGaO[34] and 1.45 for the cap material. Periodic boundary conditions were employed. The simulation results are shown in Figure 3b. In the simulation, a perfectly symmetric structure was assumed, which leads to identical results for both orthogonal input polarizations. For calculations performed at normal incidence, we can identify two resonances at 890 and 1030 nm. However, the resonance at 970 nm could not be excited in the simulations that assume normal incidence plane-wave excitation. Thus, in order to emulate the effect of excitation with a finite NA as used in the experiment, we furthermore performed simulations with tilted plane-wave excitation (incident angle β). This allowed us to excite the additional resonance in the simulations. Since this mode is

DOI: 10.1021/acsphotonics.7b01533
ACS Photonics 2018, 5, 1786−1793

symmetry-forbidden under normal-incidence excitation, it is here referred to as "symmetry-forbidden mode" (SM). Such modes were previously described for plasmonics[38] and for dielectric metasurfaces.[39] Note that the spectral position and strength of the SM depend on the incidence angle.

The near-field distributions for the three resonances are visualized in Figure 3c–e only for close-ups of the GaAs disks, where the observed fields are much stronger than in the other layers. Based on these, we can identify the resonance at 890 nm as the electric dipole (ED) resonance and the one at 1030 nm as the magnetic dipole (MD) resonance of the nanocylinders. The field distribution of the SM resonance is more complicated, pointing toward a hybrid-mode character with contributions from several multipolar orders.

We also performed linear-optical measurements and simulations for the SH wavelengths. Due to the high absorption of GaAs in this spectral domain, no well-defined resonances could be identified.

Experimental Investigation of SHG Polarization Dependence. Next, in order to investigate the polarization dependence of the generated SH, we performed second harmonic Fourier imaging using a home-built setup. A sketch of the setup is shown in Figure 4a. The sample is excited by a

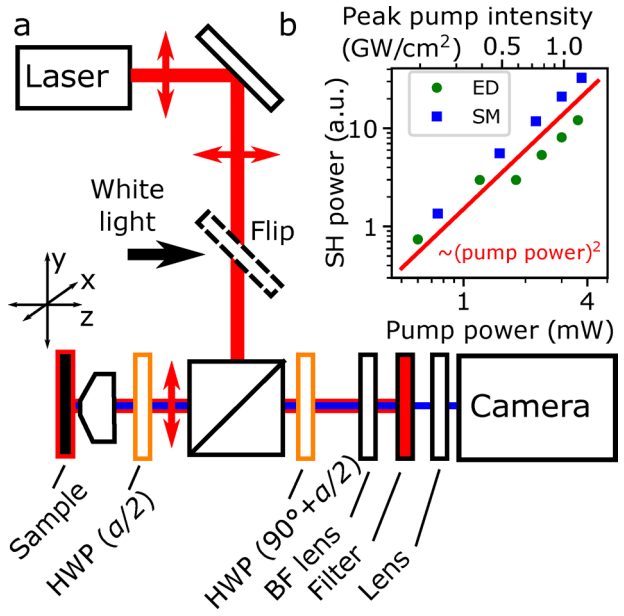

Figure 4. (a) Sketch of the setup used for second-harmonic Fourier imaging. (b) Measured SH power for ED (green dots) and SM (blue squares) resonances in dependence on the FH input power. The expected quadratic dependence of the SH power is indicated as a guide for the eye by the red line.

pulsed tunable Ti:sapphire laser (Spectra Physics - MaiTai HP DeepSee) with pulse durations around 100 fs. The laser beam is brought to the sample by a 90:10 nonpolarizing beam splitter (Thorlabs BS025) and focused onto the sample by a microscope objective (Zeiss 100×/0.75 epiplan) with a numerical aperture of NA = 0.75. By adjusting the excitation beam diameter to underfill the entrance pupil of the microscope objective, we reduce the excitation NA to obtain an FH spot-size of about 7 μm diameter, thus exciting on average about 9 × 9 nanocylinders in the metasurface. The generated SH is collected making use of the full NA of the microscope objective to collect all propagating diffraction orders, namely the zeroth and the first orders. The reflected FH is filtered out by a short-pass filter, while the spatial spectrum of the SH at the back focal (BF) plane of the microscope objective is imaged onto an electron-multiplying CCD camera (Andor iXon3 EMCCD) using an additional lens (Thorlabs LA1708, focal length 200 mm, 1 in. diameter) in a 2f geometry (BF-lens in Figure 4a). Alignment of the BF lens was performed using a blue laser with emission wavelength of 473 nm close to the SH wavelength. The distance between sample and Fourier plane is ∼25 cm. This allows us to separately analyze the SHG signal emitted into the different diffraction orders due to the periodic arrangement in the metasurface. We control the FH polarization via a half-wave plate (HWP, Thorlabs AHWP05M-980) behind the last reflecting optical element in front of the sample. This way, we avoid different phase additions for the TE and TM polarized components of the FH in the reflecting beamsplitter and mirrors, which would lead to elliptical polarization states of the FH. The retardation of the SH light accumulated by passing through this HWP at angle $\alpha/2$ is compensated by a second identical HWP oriented at angle (90° + $\alpha/2$) in the detection path.

As a first set of nonlinear measurements, we confirm that we indeed observe SHG by measuring the quadratic power dependence of the generated light. Figure 4b shows the SH power obtained by integrating all counts within one frame of the CCD-camera as a function of the FH input power. The excitation wavelength was subsequently tuned to 940 and 1020 nm wavelength to excite the metasurface at its electric dipole resonance and the symmetry-forbidden resonance, respectively. Note that in these measurements, a sample with slightly bigger dimensions was used in order to avoid the risk of structural damage of our primary sample for high excitation powers. For this sample, the MD resonance occurs beyond the tuning range of our laser and could thus not be excited. For both measured resonances, we find the expected quadratic increase of the measured signal with the FH power.

The results of the second-harmonic nonlinear Fourier imaging measurements are summarized in Figure 5. Figure 5a,b shows two exemplary momentum-space intensity distributions of the generated SH light for x-polarized excitation at the ED and SM resonance, respectively. At the SH wavelength, the metasurface behaves like a grating, channeling the emission into the directions defined by diffraction. As governed by the ratio of lattice periodicity and wavelength, only the zeroth and first diffraction orders are propagating modes, while higher orders remain evanescent. Importantly, Figure 5a clearly shows a vanishing zeroth diffraction order in the center (region marked by the black square), such that most of the SH light is emitted into the first orders in the x- and y-directions, marked by red and blue squares, respectively. The dashed white circle indicates the NA of the objective. The white crosses in (b) provide the positions of the diffraction orders calculated by applying the diffraction condition to our periodic arrangement.

The vanishing zeroth order of the ED resonance is in agreement with previous works on single AlGaAs nanocylinders,[31,40] showing vanishing emission in the direction normal to the substrate plane. This phenomenon can be explained by the symmetry of the nanocylinders in combination with the structure of the AlGaAs nonlinear susceptibility tensor, which is identical to that of GaAs. Here, for FH polarization along the x- or y-directions, fields along the two different in-plane axes of GaAs are excited in the metasurface, leading to SHG which is mostly polarized along the z-direction and,

DOI: 10.1021/acsphotonics.7b01533
ACS Photonics 2018, 5, 1786–1793

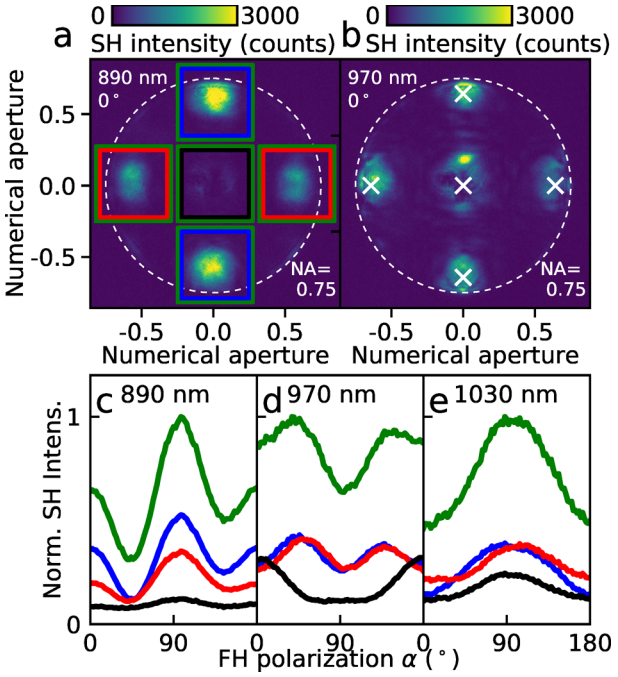

Figure 5. (a, b) Typical Fourier space SH intensity distributions measured by the CCD camera, showing the zeroth diffraction order in the center and the first orders in the *x*- and *y*-directions. The colored frames in (a) indicate the areas over which the intensities in the different orders were integrated. The large dashed white circle indicates the numerical aperture (NA) of our collecting objective. The white crosses in (b) show the positions of the diffraction orders calculated by the diffraction law. (c–e) Measured SH intensities as a function of the input polarization of the FH excitation for (c) the ED resonance at 890 nm FH wavelength, (d) the SM resonance at 970 nm, and (e) the MD resonance at 1030 nm. Curves for the different diffraction orders are color coded to the rectangles in (a), i.e., black for the zeroth diffraction order, red for the first order in *x*-direction, blue for the first order in *y*-direction, and green for all orders combined.

therefore, not propagating normal to the substrate plane. In contrast, Figure 5b shows a nonvanishing zeroth order SH for *x*-polarized excitation at the SM resonance. This may be explained by a break of the condition leading to a vanishing zeroth diffraction order due to the unintentional asymmetry of the structure evident from the polarization dependence of the linear reflection spectra. Note, however, that the SEM images and FIB cross sections do not show any obvious structural asymmetries. Thus, we cannot unambiguously assign the observed polarization dependence of the linear-optical response to any particular type of asymmetry, but have to consider various possibilities, including e.g. asymmetries in the tilt of the side walls and higher-order deviations from a circular pillar cross section. While our results indicate that zeroth order SH emission can be achieved from a GaAs metasurface, this effect and its dependence on structural asymmetries will require further investigation, e.g. by introducing a controlled symmetry break in the structure. Interestingly, for dielectric Fano-resonant metasurfaces in the linear-optical regime asymmetry was already shown to allow for low-NA normal incidence coupling to modes with out-of-plane dipole moments.[39]

Finally, to study the polarization dependence of the generated SH, we measure the SH diffraction patterns at the three resonances as a function of the FH input polarization. We obtain the SH intensities of the different orders by integrating over the areas enclosed by the colored squares, where we average contributions from the +first and −first orders in the *x*- and *y*-directions, respectively. The overall SH intensity is provided as the sum of all orders (the corresponding integration area is indicated by the green squares). Figure 5c–e shows the measured SH intensities for the different resonant excitation wavelengths and as a function of the FH polarization. The curves for the diffraction orders are color-coded to match those of the squares in Figure 5a.

The results for the ED resonance at an FH wavelength of 890 nm are shown in Figure 5c. In this case, for all diffraction orders with a non-negligible SHG signal, and correspondingly also for the total signal, the strongest SHG is observed for FH polarizations along the symmetry axes of the metasurface, that is, for an inclination of 45° with respect to the equivalent (010)- and (001)-crystalline axes of GaAs (see Figure 1c). This behavior is in accordance with previous studies performed for single III–V semiconductor nanocylinders and with the structure of the nonlinear tensor of the GaAs, which permits only nonlinear interactions involving three differently oriented field components.

A qualitatively different behavior can be observed at the SM resonance, plotted in Figure 5d. Here, the largest total SH emission is found for FH polarizations along the GaAs crystal axes, that is, oriented at 45° with respect to the symmetry axes of the metasurface. A similar FH polarization dependence is found for SH emission into the first diffraction orders. The zeroth diffraction order, on the other hand, shows a significant intensity for *x*-polarized FH excitation only. The nominal symmetry of the metasurface with respect to 90° changes of the FH polarization is broken in this zeroth diffraction order, an effect which was already noted in the linear reflection spectra. We find the FH polarization dependence of the SHG at the MD resonance (see Figure 5e) to be dominated by this symmetry break, exhibiting only one maximum for *y*-polarized FH excitation in each diffraction order as well as in the total signal.

Qualitatively the same results could be measured on a sample with slightly bigger dimensions (see Supporting Information).

Our results demonstrate that control of the FH polarization allows for tuning the SH response of resonant GaAs metasurfaces, where the polarization dependence of the generated SH itself can be tailored by the resonance properties of the metasurface. Surprisingly, this includes a case where the maximum SHG efficiency is achieved for excitation along the crystalline axis of GaAs, which would not be possible in unstructured bulk GaAs due to the specific nonlinear tensor structure of this material.

Simulation of SHG Polarization Dependence. To qualitatively reproduce and explain our experimental findings, we extend our linear finite-element simulations of the GaAs metasurfaces to the nonlinear-optical regime using the undepleted pump approximation. To simulate SHG by the metasurface, the electric near field excited by the incident FH plane wave is used to calculate the induced nonlinear polarization in the nanocylinders as

$$P_i^{\mathrm{NL}}(2\omega) = \epsilon_0 \sum_j \sum_k \chi_{ijk}^{(2)} E_j^{\mathrm{FH}}(\omega) E_k^{\mathrm{FH}}(\omega) \quad (1)$$

where the nonlinear tensor has only elements coupling all three polarization directions. The resulting nonlinear polarization is used as a source term at the SH frequency for computing SH

DOI: 10.1021/acsphotonics.7b01533
ACS Photonics 2018, 5, 1786–1793

field propagation in a second set of simulations (see Methods section).

Note that our model captures a simplified, idealized version of the experimental sample only. As already the case for the linear-optical simulations, the individual constituents of the metasurface are modeled as rotationally symmetric cylinders. Consequently, the anisotropy observed in the linear and nonlinear polarization-resolved spectroscopy is not reproduced. Furthermore, the nonlinear simulations assume normal-incidence plane-wave excitation, thus limiting the analysis to the excitable ED and MD resonances. The intensities of the calculated SH diffraction orders for excitation at the ED (MD) resonance at 890 nm (1030 nm), are shown in Figure 6a,b as a function of α. The zeroth order has zero intensity in all simulations due to the symmetry of the metasurface and the structure of the nonlinear tensor.[31] For the other diffraction orders (red and blue lines) and the total emitted SH (green lines), the two resonances show a qualitatively different behavior. The SH generated at the ED resonance in Figure 6a has its maxima at input polarizations along the metasurface symmetry axes, in accordance with our measurement results. This is expected,[11,31,40] as the electric dipole mode is characterized by linear electric field components inside the nanocylinders which are predominantly oriented in the direction of the incident polarization, and since the nonlinear tensor of GaAs permits only nonlinear interactions involving three differently oriented field components. For FH polarization along the x- or y-directions, fields along both in-plane crystal axes of GaAs are excited in the metasurface, creating a z-polarized dipolar nonlinear polarization leading to SHG emission in the first diffraction orders. Other components of the nonlinear polarization corresponding to higher-order (Mie-type) modes are also excited but do not significantly contribute to SHG radiation. For FH polarizations with $\alpha = 45°$, predominantly fields along only one in-plane crystal axis of GaAs are excited, suppressing the z-polarized nonlinear polarization. As again the induced other components of the nonlinear polarization do not significantly contribute to SHG radiation, much less SH than for $\alpha = 0°$ is emitted.

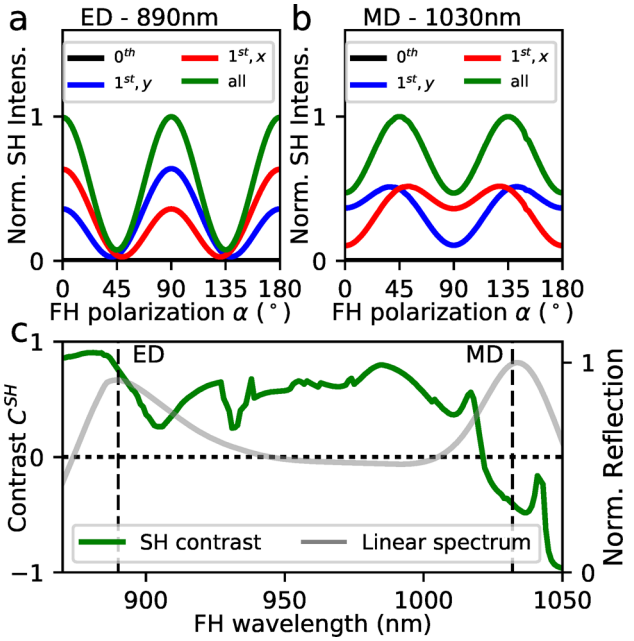

Figure 6. (a, b) Numerical simulation of SH intensities depending on the input polarization of the FH excitation for (a) the ED resonance at 890 nm FH wavelength and (b) the MD resonance at 1030 nm for the zeroth diffraction order (black), first order in x-direction (red), first order in y-direction (blue), and all orders combined (green). (c) Spectral dependence of the SH contrast C^{SH} for the overall SH intensity (green, see eq 1). The simulated linear reflection spectrum is plotted in gray for reference.

In contrast to this, the SH excited at the MD resonance in Figure 6b has higher intensities at $\alpha = 45°$ and 135°. This qualitatively reproduces the behavior we found in our measurements at the SM resonance, although these are two different resonances. Our simulations show, however, that this nonintuitive behavior can be found also in metasurfaces with circularly symmetric constituents and is not only caused by the asymmetry of the experimental structures. The possibility of nonzero SHG for FH polarizations along the in-plane crystal axes can be explained by the more complex local field structure of the magnetic and symmetry-forbidden resonances at the FH frequency, allowing fields to be excited along more than a single crystal axis of GaAs.

The transition between maximum SHG at the metasurface symmetry axes and at the GaAs crystal axes is visualized in Figure 6c, where we plot the contrast between the integrated SH intensities emitted at $\alpha = 0°$ and 45° FH polarization angles

$$C^{SH} = \frac{I_0^{SH} - I_{45}^{SH}}{I_0^{SH} + I_{45}^{SH}} \tag{2}$$

The contrast C^{SH}, plotted with the green line in Figure 6c together with the simulated linear reflection spectrum in gray as a function of the FH wavelength, is positive for wavelengths below 1000 nm. This corresponds to the spectral region where the nonlinear excitation is dominated by resonant (around the ED resonance) or off-resonant (in between the two resonances) electric dipolar response at the FH wavelength. Here, the maximum SH is generated for FH polarizations of $\alpha = 0°$ or 90° FH polarization angle. For wavelengths close to the magnetic resonance, the contrast becomes negative, indicating maximum SH generation for FH excitation along the GaAs crystal axis at $\alpha = 45°$. The change of sign of the contrast C^{SH} and with it the change of polarization-dependence only occurs when the MD dominates over the ED. This underpins that the polarization dependence can be reversed with respect to the unstructured bulk material and ED resonance by the use of resonances with nontrivial electric near-field profiles.

CONCLUSION

In summary, we investigated the spatial emission properties and the dependence on the polarization of the pump of SHG from a homogeneous Mie-resonant GaAs metasurface. We find that SHG is predominantly emitted into the first diffraction orders of the periodic array. Furthermore, we show that the type of resonance excited at the FH frequency has a strong influence on the FH polarization angle, for which the maximum SHG is observed. Most notably, we demonstrate that for resonances with a complex near-field structure, an FH polarization along the crystal axis of GaAs, for which SHG would be forbidden on an unstructured GaAs surface, can become the preferential excitation polarization direction. All these observations were verified by finding qualitative correspondence of our experimental results with numerical simulations of SHG emitted by the metasurface structure. All in all, our work provides new

DOI: 10.1021/acsphotonics.7b01533
ACS Photonics 2018, 5, 1786−1793

insights for identifying the relevant optimization parameters for the development of efficient nonlinear metasurfaces with a pump-polarization-sensitive and directionally tailored optical response. In particular, the importance of the spatial lattice of the metasurface and of the intrinsic semiconductor crystal structure on the properties of generated nonlinear fields is demonstrated. Finally, they also shed new light on the important role the collecting optics play in nonlinear experiments with metasurfaces.

METHODS

Sample Fabrication. The investigated sample consists of a periodic array of multilayered pillars (see Figure 2a) fabricated as described in Reference.[12] On the GaAs substrate, a ∼300 nm thick $Al_{0.85}Ga_{0.15}As$ layer followed by a ∼300 nm thick GaAs layer is formed via molecular beam epitaxial growth. This stack is covered by a resist layer (HSQ Fox-16), which is patterned by electron-beam lithography and developed to form ∼500 nm thick SiO_2 disks which are then used as a mask for chlorine-based inductively coupled-plasma etching. Finally, a selective wet oxidation process converts the $Al_{0.85}Ga_{0.15}As$ into $(Al_xGa_{1-x})_2O_3$. Removal of the cap layer without affecting the oxide disk is difficult. However, owing to the large refractive index difference between GaAs (n = 3.5) and SiO_2 (n = 1.4), the cap does not have a detrimental effect on the metasurface resonance properties. For our sample, we furthermore obtain a GaAs pedestal originating from overetching.

The final result for our fabricated sample shows a diameter of 244 nm for both the GaAs and $(Al_xGa_{1-x})_2O_3$ disks, while the height differs from 290 to 280 nm, respectively. The diameter of the pedestal decreases from the oxide cylinder to around 235 nm and increases again to the substrate with a wide diameter of around 500 nm (see Figure 2b). Its overall height is around 290 nm. The cap is slightly bigger than the rest of the pillar with a diameter of 296 nm and a height of 470 nm.

The two in-plane crystal axes of the GaAs are rotated for 45° with respect to the two axes of the rectangular array of the pillars. The third crystal axis is normal to the surface.

SHG Simulation. For the SHG simulation, we use an adaptive higher-order finite-element method[35] implemented in the commercial solver "JCMsuite".[36] As a source for the bulk SH calculation, we use a current density in the GaAs cylinder resulting from the nonlinear polarization according to the $\chi^{(2)}$-tensor ($\chi^{(2)}_{ijk}$ = 740 pm/V for $i \neq j \neq k$ otherwise zero)[30] and the fields generated in the GaAs cylinder by the FH plane wave:

$$j_i(2\omega) = -i2\omega P_i^{\mathrm{NL}}(2\omega) = -i2\omega\epsilon_0 \sum_{jk} \chi^{(2)}_{ijk} E_j(\omega) E_k(\omega) \tag{3}$$

ASSOCIATED CONTENT

Supporting Information

The Supporting Information is available free of charge on the ACS Publications website at DOI: 10.1021/acsphotonics.7b01533.

Second-harmonic Fourier imaging and input-polarization dependent measurements performed on a similar sample with slightly bigger dimensions, showing qualitatively the same results (Figures S1 and S2). Additional simulation for a sample with slightly tilted pillars (Figures S3 and S4) (PDF).

AUTHOR INFORMATION

Corresponding Author

*E-mail: franz.loechner@uni-jena.de.

ORCID

Franz J. F. Löchner: 0000-0002-8003-7916
Sheng Liu: 0000-0001-5644-7715
Andrey A. Fedyanin: 0000-0003-4708-6895
Igal Brener: 0000-0002-2139-5182

Notes

The authors declare no competing financial interest.

ACKNOWLEDGMENTS

We thank M. Steinert and S. Fasold for help with FIB milling and SEM imaging. Financial support by the Thuringian State Government within its ProExcellence initiative (ACP[2020]), by the German Research Foundation (STA 1426/2-1) and by Einstein Foundation Berlin (ECMath-OT9) is gratefully acknowledged. F.L. has been funded by the German Research Foundation (DFG) through the International Research Training Group (IRTG) 2101. A.F. was funded by the German Academic Exchange Service (DAAD) via the program Ostpartnerschaften and the Graduate School Scholarship Programm (GSSP). Parts of this work were supported by the U.S. Department of Energy, Office of Basic Energy Sciences, Division of Materials Sciences and Engineering and performed, in part, at the Center for Integrated Nanotechnologies, an Office of Science User Facility operated for the U.S. Department of Energy (DOE) Office of Science. Sandia National Laboratories is a multimission laboratory managed and operated by National Technology and Engineering Solutions of Sandia, LLC, a wholly owned subsidiary of Honeywell International, Inc., for the U.S. Department of Energy's National Nuclear Security Administration under contract DE-NA-0003525. F.S. is funded by the German Federal Ministry of Education and Research within the Zwanzig20 consortium 3D sensation (FKZ 03ZZ0434).

REFERENCES

(1) Kuznetsov, A. I.; Miroshnichenko, A. E.; Brongersma, M. L.; Kivshar, Y. S.; Luk'yanchuk, B. Optically resonant dielectric nanostructures. *Science* **2016**, *354*, aag2472.

(2) Staude, I.; Schilling, J. Metamaterial-inspired silicon nanophotonics. *Nat. Photonics* **2017**, *11*, 274−284.

(3) Decker, M.; Staude, I.; Falkner, M.; Dominguez, J.; Neshev, D. N.; Brener, I.; Pertsch, T.; Kivshar, Y. S. High-Efficiency Dielectric Huygens' Surfaces. *Adv. Opt. Mater.* **2015**, *3*, 813−820.

(4) Chong, K. E.; Staude, I.; James, A.; Dominguez, J.; Liu, S.; Campione, S.; Subramania, G. S.; Luk, T. S.; Decker, M.; Neshev, D. N.; Brener, I.; Kivshar, Y. S. Polarization-Independent Silicon Metadevices for Efficient Optical Wavefront Control. *Nano Lett.* **2015**, *15*, 5369−5374.

(5) Chong, K. E.; Wang, L.; Staude, I.; James, A. R.; Dominguez, J.; Liu, S.; Subramania, G. S.; Decker, M.; Neshev, D. N.; Brener, I.; Kivshar, Y. S. Efficient polarization insensitive complex wavefront control using Huygens' metasurfaces based on dielectric resonant meta-atoms. *ACS Photonics* **2016**, *3*, 514−519.

(6) Yu, Y. F.; Zhu, A. Y.; Paniagua-Dominguez, R.; Fu, Y. H.; Luk'yanchuk, B.; Kuznetsov, A. I. High-transmission dielectric metasurface with 2π phase control at visible wavelenghts. *Laser Photonics Rev.* **2015**, *9*, 412−418.

(7) Shcherbakov, M. R.; Neshev, D. N.; Hopkins, B.; Shorokhov, A. S.; Staude, I.; Melik-Gaykazyan, E. V.; Decker, M.; Ezhov, A. A.; Miroshnichenko, A. E.; Brener, I.; Fedyanin, A. A.; Kivshar, Y. S.

DOI: 10.1021/acsphotonics.7b01533
ACS Photonics 2018, 5, 1786−1793

Enhanced Third-Harmonic Generation in Silicon Nanoparticles Driven by Magnetic Response. *Nano Lett.* **2014**, *14*, 6488−6492.
(8) Shcherbakov, M. R.; Shorokhov, A. S.; Neshev, D. N.; Hopkins, B.; Staude, I.; Melik-Gaykazyan, E. V.; Ezhov, A. A.; Miroshnichenko, A. E.; Brener, I.; Fedyanin, A. A.; Kivshar, Y. S. Nonlinear Interference and Tailorable Third-Harmonic Generation from Dielectric Oligomers. *ACS Photonics* **2015**, *2*, 578−582.
(9) Yang, Y.; Wang, W.; Boulesbaa, A.; Kravchenko, I. I.; Briggs, D. P.; Puretzky, A.; Geohegan, D.; Valentine, J. Nonlinear Fano-Resonant Dielectric Metasurfaces. *Nano Lett.* **2015**, *15*, 7388−7393.
(10) Gili, V. F.; Carletti, L.; Locatelli, A.; Rocco, D.; Finazzi, M.; Ghirardini, L.; Favero, I.; Gomez, C.; Lemaître, A.; Celebrano, M.; De Angelis, C.; Leo, G. Monolithic AlGaAs second-harmonic nanoantennas. *Opt. Express* **2016**, *24*, 15965−15971.
(11) Camacho-Morales, R.; et al. Nonlinear Generation of Vector Beams From AlGaAs Nanoantennas. *Nano Lett.* **2016**, *16*, 7191−7197.
(12) Liu, S.; Sinclair, M. B.; Saravi, S.; Keeler, G. A.; Yang, Y.; Reno, J.; Peake, G. M.; Setzpfandt, F.; Staude, I.; Pertsch, T.; Brener, I. Resonantly Enhanced Second-Harmonic Generation Using III−V Semiconductor All-Dielectric Metasurfaces. *Nano Lett.* **2016**, *16*, 5426−5432.
(13) Timpu, F.; Sergeyev, A.; Hendricks, N. R.; Grange, R. Second-Harmonic Enhancement with Mie Resonances in Perovskite Nanoparticles. *ACS Photonics* **2017**, *4*, 76−84.
(14) Shcherbakov, M. R.; Vabishchevich, P. P.; Shorokhov, A. S.; Chong, K. E.; Choi, D.-Y.; Staude, I.; Miroshnichenko, A. E.; Neshev, D. N.; Fedyanin, A. A.; Kivshar, Y. S. Ultrafast All-Optical Switching with Magnetic Resonances in Nonlinear Dielectric Nanostructures. *Nano Lett.* **2015**, *15*, 6985−6990.
(15) Della Valle, G.; Hopkins, B.; Ganzer, L.; Stoll, T.; Rahmani, M.; Longhi, S.; Kivshar, Y. S.; De Angelis, C.; Neshev, D. N.; Cerullo, G. Nonlinear anisotropic dielectric metasurfaces for ultrafast nanophotonics. *ACS Photonics* **2017**, *4*, 2129.
(16) Marino, G.; Solntsev, A. S.; Xu, L.; Gili, V.; Carletti, L.; Poddubny, A. N.; Smirnova, D.; Chen, H.; Zhang, G.; Zayats, A. V.; De Angelis, C.; Leo, G.; Kivshar, Y.; Sukhorukov, A.; Neshev, D. N. Sum-Frequency Generation and Photon-Pair Creation in AlGaAs Nano-Scale Resonators. *Conference on Lasers and Electro-Optics* **2017**, FTu4D.2.
(17) Liu, S.; Vabishchevich, P. P.; Vaskin, A.; Reno, J. L.; Keeler, G. A.; Sinclair, M. B.; Staude, I.; Brener, I. An optical metamixer. *arXiv:1711.00090 [physics.optics]*, **2017**.
(18) Liu, H.; Guo, C.; Vampa, G.; Zhang, J. L.; Sarmiento, T.; Xiao, M.; Bucksbaum, P. H.; Vučković, J.; Fan, S.; Reis, D. A. Enhanced High-Harmonic Generation from an All-Dielectric Metasurface. *arXiv:1710.04244 [physics.optics]*, **2017**
(19) Grinblat, G.; Li, Y.; Nielsen, M. P.; Oulton, R. F.; Maier, S. A. Degenerate Four-Wave Mixing in a Multiresonant Germanium Nanodisk. *ACS Photonics* **2017**, *4*, 2144−2149.
(20) Shcherbakov, M. R.; Liu, S.; Zubyuk, V. V.; Vaskin, A.; Vabishchevich, P. P.; Keeler, G.; Pertsch, T.; Dolgova, T. V.; Staude, I.; brener, I.; Fedyanin, A. A. Ultrafast all-optical tuning of direct-gap semiconductor metasurfaces. *Nat. Commun.* **2017**, *8*, 17.
(21) Shcherbakov, M. R.; Werner, K.; Fan, Z.; Talisa, N.; Chowdhury, E.; Shvets, G. Non-integer harmonics generation by photon acceleration in rapidly evolving nonlinear semiconductor metasurfaces. *arXiv:1710.06966 [physics.optics]*, 2017.
(22) Segal, N.; Keren-Zur, S.; Hendler, N.; Ellenbogen, T. Controlling light with metamaterial-based nonlinear photonic crystals. *Nat. Photonics* **2015**, *9*, 180−184.
(23) Tymchenko, M.; Gomez-Diaz, J. S.; Lee, J.; Nookala, N.; Belkin, M. A.; Alù, A. Gradient Nonlinear Pancharatnam-Berry Metasurfaces. *Phys. Rev. Lett.* **2015**, *115*, 207403.
(24) Kauranen, M.; Zayats, A. V. Nonlinear Plasmonics. *Nat. Photonics* **2012**, *6*, 737−748.
(25) Chen, R.; Crankshaw, S.; Tran, T.; Chuang, L. C.; Moewe, M.; Chang-Hasnain, C. Second-harmonic generation from a single wurtzite GaAs nanoneedle. *Appl. Phys. Lett.* **2010**, *96*, 051110.
(26) Timofeeva, M.; Bouravleuv, A.; Cirlin, G.; Shtrom, I.; Soshnikov, I.; Escale, M. R.; Sergeyev, A.; Grange, R. Polar Second-Harmonic Imaging to Resolve Pure and Mixed Crystal Phases along GaAs Nanowires. *Nano Lett.* **2016**, *16*, 6290−6297.
(27) Pimenta, A. C. S.; Teles Ferreira, D. C.; Roa, D. B.; Moreira, M. V. B.; de Oliveira, A. G.; González, J. C.; De Giorgi, M.; Sanvitto, D.; Matinaga, F. M. Linear and Nonlinear Optical Properties of Single GaAs Nanowires with Polytypism. *J. Phys. Chem. C* **2016**, *120*, 17046−17051.
(28) Liu, S.; Keeler, G. A.; Reno, J. L.; Sinclair, M. B.; Brener, I. III−V semiconductor nanoresonators − A new strategy for passive, active, and nonlinear all-dielectric metamaterials. *Adv. Opt. Mater.* **2016**, *4*, 1457−1462.
(29) Cambiasso, J.; Grinblat, G.; Li, Y.; Rakovich, A.; Cortés, E.; Maier, S. A. Bridging the Gap between Dielectric Nanophotonics and the Visible Regime with Effectively Lossless Gallium Phosphide Antennas. *Nano Lett.* **2017**, *17*, 1219−1225.
(30) Boyd, R. W. *Nonlinear Opt.*, 3rd ed.; Academic Press, 2008.
(31) Carletti, L.; Locatelli, A.; Neshev, D.; De Angelis, C. Shaping the Radiation Pattern of Second-Harmonic Generation from AlGaAs Dielectric Nanoantennas. *ACS Photonics* **2016**, *3*, 1500−1507.
(32) Ghirardini, L.; Carletti, L.; Gili, V.; Pellegrini, G.; Duò, L.; Finazzi, M.; Rocco, D.; Locatelli, A.; De Angelis, C.; Favero, I.; Ravaro, M.; Leo, G.; Lemaître, A.; Celebrano, M. Polarization properties of second-harmonic generation in AlGaAs optical nanoantennas. *Opt. Lett.* **2017**, *42*, 559−562.
(33) Rahmani, M.; Shorokhov, A. S.; Hopkins, B.; Miroshnichenko, A. E.; Shcherbakov, M. R.; Camacho-Morales, R.; Fedyanin, A. A.; Neshev, D. N.; Kivshar, Y. S. Nonlinear Symmetry Breaking in Symmetric Oligomers. *ACS Photonics* **2017**, *4*, 454−461.
(34) Choquette, K. D.; Geib, K. M.; Ashby, C. I.; Twesten, R. D.; Blum, O.; Hou, H. Q.; Follstaedt, D. M.; Hammons, B. E.; Mathes, D.; Hull, R. Advances in selective wet oxidation of AlGaAs alloys. *IEEE J. Sel. Top. Quantum Electron.* **1997**, *3*, 916−926.
(35) Pomplun, J.; Burger, S.; Zschiedrich, L.; Schmidt, F. Adaptive finite element method for simulation of optical nano structures. *Phys. Status Solidi B* **2007**, *244*, 3419−3434.
(36) JCMwave, *FEM solver JCMsuite*, Version 3.4, www.jcmwave.com.
(37) Palik, E. D. *Handbook of Optical Constants of Solids*; Academic press, 1997; Vol. *I*; pp 429−443.
(38) Enkrich, C.; Wegener, M.; Linden, S.; Burger, S.; Zschiedrich, L.; Schmidt, F.; Zhou, J. F.; Koschny, T.; Soukoulis, C. M. Magnetic Metamaterials at Telecommunication and Visible Frequencies. *Phys. Rev. Lett.* **2005**, *95*, 203901.
(39) Campione, S.; Liu, S.; Basilio, L. I.; Warne, L. K.; Langston, W. L.; Luk, T. S.; Wendt, J. R.; Reno, J. L.; Keeler, G. A.; Brener, I.; Sinclair, M. B. Broken Symmetry Dielectric Resonators for High Quality Factor Fano Metasurfaces. *ACS Photonics* **2016**, *3*, 2362−2367.
(40) Carletti, L.; Locatelli, A.; Stepanenko, O.; Leo, G.; De Angelis, C. Enhanced second-harmonic generation from magnetic resonance in AlGaAs nanoantennas. *Opt. Express* **2015**, *23*, 26544−26550.

DOI: 10.1021/acsphotonics.7b01533
ACS Photonics 2018, 5, 1786−1793